HIGH PERFORMANCE PIAA CORONAGRAPHY WITH COMPLEX AMPLITUDE FOCAL PLANE MASKS

OLIVIER GUYON[1,2], FRANTZ MARTINACHE[1], RUSLAN BELIKOV[3], AND REMI SOUMMER[4]
[1] National Astronomical Observatory of Japan, Subaru Telescope, Hilo, HI 96720, USA; guyon@naoj.org
[2] Steward Observatory, University of Arizona, Tucson, AZ 85721, USA
[3] NASA Ames Research Center, Mail Stop 204-2, Moffett Field, CA 94035, USA
[4] Space Telescope Science Institute, 3700 San Martin Drive, Baltimore, MD 21218-2463, USA
Received 2009 October 23; accepted 2010 July 29; published 2010 September 16

ABSTRACT

We describe a coronagraph approach where the performance of a Phase-Induced Amplitude Apodization (PIAA) coronagraph is improved by using a partially transmissive phase-shifting focal plane mask and a Lyot stop. This approach combines the low inner working angle offered by phase mask coronagraphy, the full throughput and uncompromised angular resolution of the PIAA approach, and the design flexibility of Apodized Pupil Lyot Coronagraph. A PIAA complex mask coronagraph (PIAACMC) is fully described by the focal plane mask size, or, equivalently, its complex transmission which ranges from 0 (opaque) to -1 (phase shifting). For all values of the transmission, the PIAACMC theoretically offers full on-axis extinction and 100% throughput at large angular separations. With a pure phase focal plane mask (complex transmission $= -1$), the PIAACMC offers 50% throughput at $0.64\,\lambda/D$ while providing total extinction of an on-axis point source. This performance is very close to the "fundamental performance limit" of coronagraphy derived from first principles. For very high contrast level, imaging performance with PIAACMC is in practice limited by the angular size of the on-axis target (usually a star). We show that this fundamental limitation must be taken into account when choosing the optimal value of the focal plane mask size in the PIAACMC design. We show that the PIAACMC enables visible imaging of Jupiter-like planets at $\approx 1.2\,\lambda/D$ from the host star, and can therefore offer almost three times more targets than a PIAA coronagraph optimized for this type of observation. We find that for visible imaging of Earth-like planets, the PIAACMC gain over a PIAA is probably much smaller, as coronagraphic performance is then strongly constrained by stellar angular size. For observations at "low" contrast (below $\approx 10^8$), the PIAACMC offers significant performance enhancement over PIAA. This is especially relevant for ground-based high contrast imaging systems in the near-IR, where PIAACMC enables high contrast high efficiency imaging within $1\,\lambda/D$. Manufacturing tolerances for the focal plane mask are quantified for a few representative PIAACMC designs.

Key words: instrumentation: adaptive optics – techniques: high angular resolution

Online-only material: color figures

1. INTRODUCTION

Direct imaging of exoplanets requires optical systems able to overcome the high star-to-planet brightness ratio and the small angular separation between the two bodies. For ground-based telescopes, young massive planets, preferably on large orbits, are the most accessible targets for existing and future telescopes equipped with adaptive optics systems operating in the near-IR (Marois et al. 2008; Lagrange et al. 2009). Improvements in high contrast imaging techniques are required to allow imaging of lower mass/older planets closer in to the star. Potentially habitable planets are significantly harder to image, as they are both closer in and fainter, and imaging them will most likely require a stable space telescope equipped with a high performance coronagraph and a precise wavefront control system.

Many coronagraph system concepts have recently been proposed to image exoplanets from ground-based or space telescopes (Guyon et al. 2006). Among these numerous options, the Phase-Induced Amplitude Apodization (PIAA) coronagraph (Guyon 2003) is particularly attractive thanks to the combination of high throughput, high contrast, and small inner working angle (IWA). We present in this paper an improvement of the PIAA technique which uses a Lyot mask and a partially transmissive phase-shifting focal plane mask. The new concept is therefore named PIAA complex mask coronagraph

(PIAACMC) in this paper. The PIAACMC principle is introduced in Section 2 by combining four key techniques: apodized pupil coronagraphy, apodized pupil Lyot coronagraphy, phase mask coronagraphy, and lossless apodization with PIAA optics. The PIAACMC performance is shown in Section 3, where it is compared to the coronagraph approaches which inspired its design. The PIAACMC sensitivity to stellar angular size is discussed in Section 4, and manufacturing requirements and challenges are identified in Section 5.

2. AMPLITUDE APODIZED PUPIL CORONAGRAPHY AND PIAACMC

In this section, the coronagraph concepts leading to the PIAACMC design are introduced. Their strengths and weaknesses are described in order to discuss how they can optimally be combined, ultimately leading to the PIAACMC approach.

2.1. Entrance Pupil Apodization

Entrance Pupil Apodization with amplitude masks can produce high contrast point-spread functions (PSFs). The apodization mask, placed in the entrance pupil, can be continuous (Jacquinot & Roisin-Dossier 1964; Nisenson & Papaliolios 2001; Gonsalves & Nisenson 2003; Aime 2005) or binary (Kasdin et al. 2003; Vanderbei et al. 2003, 2004). The binary masks used in "shaped pupil" coronagraphs have the advantage
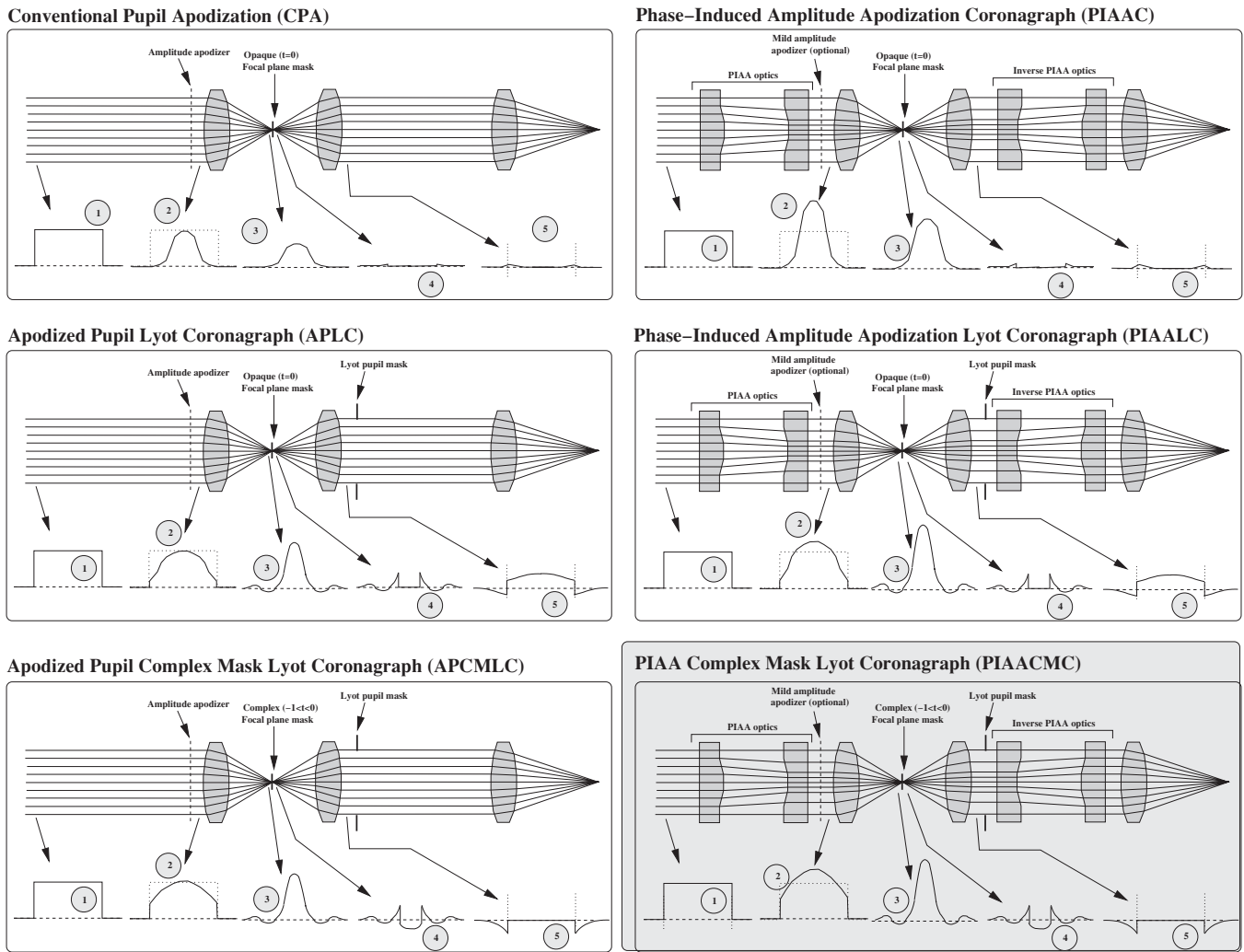
Figure 1. Coronagraphic architectures discussed in this paper. In CPA (top left), the coronagraphic effect is obtained by the combination of a pupil plane apodizer and a focal plane mask. Performance is augmented in the Apodized Pupil Lyot Coronagraph (APLC) by introducing a Lyot mask in the output pupil plane (center left). Further performance improvement is achieved by replacing the opaque focal plane occulting mask with a partially transmissive phase-shifting mask (bottom left). The right part of this figure shows the equivalent coronagraph designs when apodization is performed by lossless PIAA optics instead of a classical apodizer. A graphical representation of complex amplitude in a few relevant planes is shown for each coronagraph: (1) telescope entrance pupil, (2) pupil after apodization, (3) focal plane before introduction of the focal plane mask, (4) focal plane after the focal plane mask, and (5) exit pupil plane before truncation by the Lyot mask. The PIAA Complex Mask Lyot Coronagraph (PIAACMC), shown in the bottom right of this figure, offers the highest performance of all configurations, and its performance and design are the focus of this work.

of being achromatic and significantly easier to manufacture than continuous transmission masks. Apodization by Mach–Zehnder type pupil plane interferometry was also suggested (Aime et al. 2001) to produce a continuous apodization. For high contrast levels, the apodization becomes very strong, resulting in a low throughput and a relatively poor IWA. Pupil amplitude apodization coronagraphs are very robust, easy to implement, and very achromatic (especially for shaped pupils), but are not efficient at high contrast levels.

A conceptual layout of a conventional pupil apodization (CPA) imaging system is shown in the upper left corner of Figure 1. The telescope entrance pupil (1) is apodized with an amplitude mask to produce an apodized pupil (2) which yields a high contrast PSF (3). Prior to re-imaging on the science detector, the central part of the PSF is masked (4) with an opaque mask. While masking starlight in the focal plane and re-imaging it onto a detector is theoretically not necessary (the detector could be placed directly in the first focal plane), it

needs to be done for practical reasons since detectors have finite dynamical range.

2.2. Apodized Pupil Lyot Coronagraph

In Lyot coronagraphs, starlight is rejected by the combination of a focal plane mask and a pupil plane mask (Lyot mask) located after the focal plane mask. In the conventional Lyot coronagraph architecture, both masks are hard edged: the focal plane mask is an opaque disk blocking the central light of the PSF while the Lyot mask is a circular opening only transmitting light in the central part of the beam. This conventional architecture offers limited performance, and the radius of the focal plane mask (a smaller mask allows imaging closer to the optical axis) is traded against contrast and system throughput: the Lyot mask is undersized (smaller than the pupil) and its size becomes smaller as the focal plane mask radius is reduced. Higher coronagraphic performance can be obtained by apodizing the entrance pupil of

the Lyot coronagraph in an Apodized Pupil Lyot Coronagraph (APLC) design, where the Lyot mask does not need to be undersized, and both the apodization profile and the focal plane mask size are tuned to minimize light inside the geometric pupil but allow light outside the Lyot stop. The APLC is therefore a Lyot coronagraph with a hard-edged opaque (transmission $t = 0$) focal plane mask and an amplitude-apodized entrance aperture (Soummer et al. 2003a; Soummer 2005; Soummer et al. 2009). Soummer et al. (2003a) showed that the optimal apodization functions to for APLCs are prolate spheroidal functions.

The conceptual APLC layout, shown in Figure 1 (center, left) shows the addition of the Lyot mask in the exit pupil plane. With an APLC, starlight rejection is shared between the focal plane mask and the Lyot mask. Compared to the CPA scheme, a milder, higher throughput apodization can therefore be used, and a smaller focal plane can be used for smaller IWA.

2.3. Apodized Pupil Lyot Coronagraph with Partially Transmissive Phase-shifting Focal Plane Mask

Soummer et al. (2003a) showed that the APLC formalism can be applied to the phase mask coronagraph (focal plane mask transmission $t = -1$) proposed in Roddier & Roddier (1997) and for which a pupil apodization function providing total coronagraphic extinction was numerically derived by Guyon & Roddier (2000). Soummer et al. (2003a) mathematically proved that this apodization function is also a prolate spheroidal function.

In this section, we generalize the APLC and apodized pupil phase mask coronagraph concepts to Lyot coronagraphs using focal plane masks with negative complex amplitude transmission values $-1 < t < 0$. Such masks are partially transmissive and introduce a π phase shift. To describe these coronagraphs, we follow the APLC formalism established by Soummer et al. (2003a, 2009) and Soummer (2005).

We denote a the focal plane mask diameter, in λ/D unit. We denote $M_a(r)$ the mask shape function ($M_a(r) = 0$ if $r > a/2$ and $M_a(r) = 1$ if $r < a/2$) and t the mask complex transmission ($t = 0$ for a purely opaque mask and $t = -1$ for pure π-shifting phase mask).

The complex amplitude $\Psi_A(r)$ in the entrance pupil of the telescope, for an on-axis source, is illustrated in Figure 1 (center left, curve (2)), and is described by

$$\Psi_A(r) = P(r)\,\phi_a(r), \tag{1}$$

where $P(r)$ is the entrance pupil shape ($P(r) = 1$ inside the pupil, zero outside) and $\phi_a(r)$ is the amplitude apodization in the pupil plane. ϕ_a is the prolate spheroidal function corresponding to the focal plane mask size a. We remind the reader that these functions are the eigenfunctions of the coronagraph operator:

$$((\phi_a(r)P(r)) * \widehat{M_a(r)}) = \Lambda_a \phi_a(r) \tag{2}$$

with Λ_a being the corresponding eigenvalue and $*$ the convolution operator. A few prolate apodization functions are shown in Figure 2, which illustrates that the pupil apodization becomes stronger as the focal plane mask radius $a/2$ increases.

The complex amplitude $\Psi_B(r)$ in the coronagraph's first focal plane, is, after multiplication by the focal plane mask complex amplitude transmission $(1 - (1 - t)M(r))$:

$$\Psi_B(r) = \hat{\Psi}_A(r)\,(1 - \epsilon M_a(r)) \tag{3}$$

with $\epsilon = 1 - t$ being equal to 1 for an APLC and 2 for a phase mask coronagraph. This complex amplitude is shown in
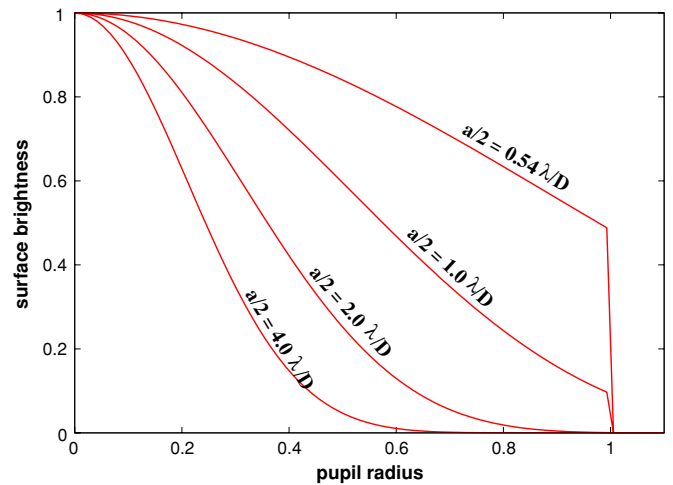

Figure 2. Prolate apodization functions for a few values of the focal plane mask radius $a/2$.

(A color version of this figure is available in the online journal.)

Figure 1, curve (4) for an APLC (center left) and for $-1 < t < 0$ (bottom left).

The complex amplitude $\Psi_C(r)$ in the Lyot plane is obtained by truncating (multiplication by the Lyot mask $P(r)$) the Fourier transform of Equation (3) and using the relationship in Equation (2):

$$\Psi_C(r) = \Psi_A(r) - \epsilon \Lambda_a \Psi_A(r). \tag{4}$$

This equation shows that the resulting complex amplitude in the Lyot plane is the coherent sum of the pupil itself ($\Psi_A(r)$) and the wave function created by the addition of the focal plane mask ($-\epsilon \Lambda_a \Psi_A(r)$).

The value of Λ_a as a function of a is given in Soummer et al. (2003a), Figure 1(A), which shows that Λ_a becomes rapidly close to 1 as a increases beyond $\approx 2\,\lambda/D$. In an APLC ($\epsilon = 1$), with a reasonably large focal plane mask ($a/2 > 1.5\,\lambda/D$), the two terms in Equation (4) almost cancel each other: a high coronagraphic extinction is reached. For example, Soummer et al. (2003a) show in Table 1 that with a focal plane mask radius equal to $1.45\,\lambda/D$ ($a = 2.9$), the integrated residual starlight is 10^{-4} for an on-axis source, and the contrast level at $3\,\lambda/D$ is 3×10^{-9}.

Equation (4) shows that the coronagraph achieves total extinction for

$$t_a = 1 - \Lambda_a^{-1}. \tag{5}$$

Since $\Lambda_a < 1$, t_a is negative. When this relationship is satisfied, the complex amplitude wave due to light outside the focal plane mask and the complex amplitude wave due to light inside the focal plane mask perfectly cancel within the geometric pupil, as shown in Figure 1, curve (5), bottom left panel.

Figure 3 shows values of Λ_a and the optimal mask transmission in intensity (t^2) as a function of the focal plane mask radius ($a/2$). For any focal plane mask radius $a/2 > 0.54\,\lambda/D$ (the exact critical value is between 0.53 and 0.54), the focal plane mask transmission t can be chosen to yield full on-axis coronagraphic extinction. At the critical value $a/2 \approx 0.54\,\lambda/D$, $\Lambda_a = 0.5$ and the focal plane mask should be fully transmissive ($t = -1$): this special case is the apodized pupil phase mask coronagraph (Roddier & Roddier 1997; Guyon & Roddier 2000; Soummer et al. 2003a), for which the pupil apodization has a 73% throughput. In this paper, we choose for numerical convenience the focal plane mask radius $a/2 = 0.54\,\lambda/D$ to represent
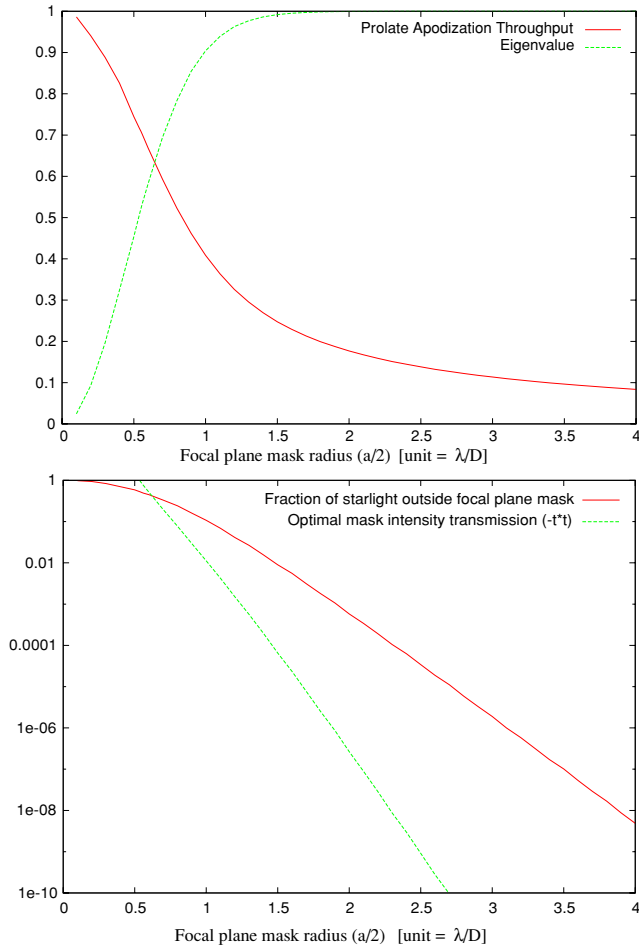
Figure 3. Top: prolate apodization function intensity throughput and eigenvalue Λ_a as a function of focal plane mask radius $a/2$. Bottom: fraction of the light outside the coronagraph focal plane mask and optimal value of the intensity transmission of the phase-shifting focal plane mask as a function of focal plane mask radius $a/2$.

(A color version of this figure is available in the online journal.)

the apodized phase mask coronagraph. This is the smallest focal plane mask radius which is a multiple of $1/100\,\lambda/D$ for which $t > -1$, and the performance of the $a/2 = 0.54\,\lambda/D$ coronagraph is very close to the mathematically ideal apodized phase mask coronagraph. This choice is due to the architecture of the numerical code used for designing the coronagraph: the radius of the focal plane mask is chosen first, and the apodization and mask transmission are then derived.

Figure 3 shows that the focal plane mask rapidly becomes opaque as its radius increases: at $a/2 = 2\,\lambda/D$ radius, t^2 should ideally be 2.7×10^{-7}, and even at the 10^{10} contrast, the coronagraph performance is identical to an apodized pupil Lyot coronagraph with a fully opaque mask. Figure 3 therefore shows that the partially transmissive phase-shifting focal plane mask introduced in this section is only useful for small focal plane mask sizes ($a/2 < 2\,\lambda/D$), when an opaque focal plane mask would fail to provide sufficiently high contrast. This point will be revisited in Section 3.3 with a more quantitative performance analysis.

2.4. Entrance Pupil Apodization with PIAA Optics: The PIAA Complex Mask Lyot Coronagraph (PIAACMC)

Phase-Induced Amplitude Apodization (PIAA) uses aspheric optics to reshape the telescope beam into an apodized beam

with no loss in throughput or angular resolution (Guyon 2003; Traub & Vanderbei 2003; Guyon et al. 2005, 2009; Vanderbei & Traub 2005; Vanderbei 2006; Martinache et al. 2006; Pluzhnik et al. 2006; Belikov et al. 2006). This coronagraphic approach, when used as a replacement for an apodizer in the CPA scheme (Figure 1, top right), offers very high performance, as it combines full throughput, small IWA, and uncompromized angular resolution. With reflective PIAA optics, chromaticity can be very low. A challenging part of this approach is the manufacturing of the aspheric optics, which often requires a "hybrid" approach where apodization is shared between a mild apodizer and PIAA optics (Pluzhnik et al. 2006). As shown in Figure 1, a set of "inverse" PIAA optics is required at the back end of the coronagraph to cancel field aberrations introduced by the first set of PIAA optics. This inverse set plays no role in the coronagraphic process, but considerably extends the field of view over which the PSF is diffraction limited.

The same lossless PIAA technique can also be used to replace the apodizer in the APLC and APCMLC configurations (Figure 1, center right and bottom right). For each coronagraph configuration shown on the left of Figure 1, the PIAA-equivalent configuration on the right removes the throughput, angular resolution, and IWA losses otherwise introduced by the apodizer. An apodized pupil complex mask Lyot coronagraph (APCMLC) configuration with a PIAA front end is especially attractive, as it combines the full throughput of the PIAA optics, the total on-axis coronagraphic extinction of the APCMLC design, and the small IWA offered by both the PIAA and the APCMLC concepts. This approach, shown in the bottom right of Figure 1, is referred to as the PIAA Complex Mask Coronagraph (PIAACMC) in this paper, and is studied in the following sections.

3. PIAACMC PERFORMANCE IN IDEAL CONDITIONS

In this section, the PIAACMC performance in ideal conditions (no manufacturing errors, perfect monochromatic wavefront, on-axis unresolved point source) is compared to the other five architectures shown in Figure 1 to illustrate and quantify the gains offered by this architecture. The goal of this section is to quantify how the Lyot mask, the complex focal plane mask, and the PIAA apodization each contribute to the coronagraph performance.

3.1. Performance Metric

Each of the six coronagraph configurations shown in Figure 1 is entirely described by the size of the focal plane mask. As discussed in Section 2.3, to each value of the mask radius $a/2$ corresponds a unique prolate apodization function ϕ_a, independently of the apodization technique (PIAA or conventional). For the APCMLC and PIAACMC configurations, the focal plane mask transmission is uniquely given by Equation (5).

The performance metric we chose to adopt is the useful throughput (UT) metric introduced by Guyon et al. (2006). The UT measures from an image containing both planet light and residual starlight how much of the planet light can be used for detection of the planet, scaled to the total amount of planet light that would be detected in a non-coronagraphic image of the planet free of starlight. At a given contrast level, the UT is defined as the amount of planet light which can be collected without collecting more residual starlight than planet light. If starlight is fully removed by the coronagraph (as this is the case for APCMC and PIAACMC coronagraphs), the UT is therefore

simply equal to the throughput for the planet light, and it will be independent of contrast between the central source and the planet. The UT will then increase from zero on the optical axis to what is commonly defined as the "coronagraph throughput" at large angular separations.

Although not perfect, this definition is quite representative of actual coronagraphic performance, as planet light which is hidden behind much brighter starlight is automatically and optimally discarded: the UT tends to properly account for planet light which can be "easily" extracted from the image. Coronagraph performance can be quickly evaluated by plotting the UT as a function of angular separation. Usual coronagraph metrics can also be accurately defined from such curves: the coronagraph throughput is the UT at large angular separation and the coronagraph IWA is the angular separation for which the curve reaches 50% of its peak value. The UT for a given coronagraph configuration is a function of the planet to star separation, the contrast level adopted, and the star angular size. The stellar angular size is considered equal to zero in this section and will be discussed in Section 4.

3.2. Useful Throughput of Several Coronagraph Configurations

Figures 4 and 5 show the UT at respectively 10^{10} and 10^6 contrast for each of the six coronagraph configurations. In each configuration, the UT is shown as a function of angular separation for a few values of the only free parameter left in the coronagraph design, the focal plane radius $a/2$. While the curves suggest that the PIAACMC offers a modest improvement over the APCMC, for both coronagraphs, small mask sizes are not realistic due to tight manufacturing tolerances and extreme sensitivity to stellar angular size. Unlike the APCMC, the PIAACMC maintains high throughput and low IWA for masks larger than $a/2 = 0.54\,\lambda/D$.

3.2.1. Conventional Pupil Apodization

At the 10^{10} contrast, pupil apodization alone does not offer high throughput or good IWA. Figure 4, upper left, shows that a strong apodization with $a/2 \approx 4.2\,\lambda/D$ is required to reach this contrast. The apodization throughput for $a/2 = 4.2\,\lambda/D$ is 8%, and the UT is therefore limited to 8% at large angular separation. With a weaker apodization ($a/2 = 3.8\,\lambda/D$), the apodization throughput is better, but the UT is smaller due to excessive stellar light leakage. With a stronger apodization ($a/2 = 5.0\,\lambda/D$), the coronagraph performance is smaller due to low throughput. The apodization strength required to reach 10^{10} contrast reduces the telescope effective size, as only light in the central part of the pupil is efficiently transmitted (Figure 2), resulting in poor angular resolution and large IWA. These limitations become less severe as the contrast goal is relaxed and a weaker apodization can be used. A $a/2 = 2.6\,\lambda/D$ apodization with a 13% throughput is sufficient to provide 10^6 contrast (Figure 5) and provides an IWA slightly smaller than $3\,\lambda/D$.

3.2.2. Apodization with PIAA Optics

With lossless apodization performed by PIAA optics, the coronagraph throughput is brought up to almost 100% and the IWA is greatly reduced thanks to full utilization of the entrance pupil. Figures 4 and 5, top right panels, show that the strength of the prolate apodization required is the same as for the conventional apodization—the only difference between the two approaches being how this apodization is performed

and what losses, if any, are created. Thanks to the lossless apodization, there is no disadvantage (other than PIAA optics manufacturing difficulty) in pushing the apodization stronger than required to reach the goal contrast. This is a fundamental difference with CPA, where doing so reduces throughput and increases the IWA. Another consequence of this behavior is that the coronagraph performance is weakly dependent on the goal contrast, as can be seen by comparing Figures 4 and 5.

3.2.3. Adding a Lyot mask: APLC and PIAALC

APLC versus CPA. By sharing the coronagraphic rejection between the focal plane mask and the Lyot mask, a weaker entrance apodization can be used at the same contrast level. The APLC performance curve in Figure 4 shows that for 10^{10} contrast, optimal coronagraph performance is reached at $a/2 = 1.8\,\lambda/D$ with a pupil plane apodization having a 20% throughput. With a larger focal plane mask, the starlight rejection is better (actually better than the required 10^{10}) but the pupil apodization is stronger and therefore reduces both throughput at large separations and IWA (more light is absorbed at the edges of the pupil, yielding a smaller effective pupil diameter). Smaller focal plane masks offer higher throughput for the planet, but fail to provide sufficiently high extinction for the central source: the UT therefore becomes lower due to increasing amounts of starlight mixed in with planet light. In the CPA configuration working at the same contrast requirement, optimal performance occurs at $a/2 = 4.2\,\lambda/D$, which corresponds to a pupil apodization with a throughput below 10%. The APLC therefore offers both higher throughput and smaller IWA thanks to the smaller focal plane mask size enabled by the use of a Lyot stop.

Figure 5 shows similar results at the 10^6 contrast, although the lower contrast allows higher throughput and a better IWA, with correspondingly smaller focal plane mask diameters.

PIAALC versus PIAA. The Lyot mask is also beneficial with a PIAA front apodization: the PIAALC performance is superior to the PIAA performance in both Figures 4 and 5. This gain is not due to the apodization itself (since PIAALC and PIAA use lossless apodization, the strength of the pupil apodization has little impact on the coronagraph performance), but to the PIAALC's ability to use an undersized focal plane mask and reject the excess light around the focal plane mask with the Lyot mask. This smaller focal plane mask offers a better IWA.

PIAALC versus APLC. In both Figures 4 and 5, direct comparison between PIAALC and APLC performances shows that PIAALC's lossless pupil apodization allows the use of apodization with larger eigenvalues (corresponding to larger values of $a/2$). In both PIAALC and APLC, the coronagraph contrast is driven by this eigenvalue, so the minimum value of $a/2$ required to achieve the required contrast is the same in both configurations ($a/2 = 1.8\,\lambda/D$ for 10^{10} contrast; $a/2 = 1.2\,\lambda/D$ for 10^6 contrast). Both coronagraphs are therefore optically identical (same apodization function, same physical focal plane mask size) except for the technique used to produce the apodized pupil. The difference is that PIAALC's lossless apodization allows the use of large eigenvalues with almost no loss in coronagraph performance, yielding full throughput and small IWA. The PIAALC curves therefore show that there is no coronagraph performance loss if the eigenvalue (or, equivalently, mask radius $a/2$) is increased beyond what is necessary to meet the contrast requirement.
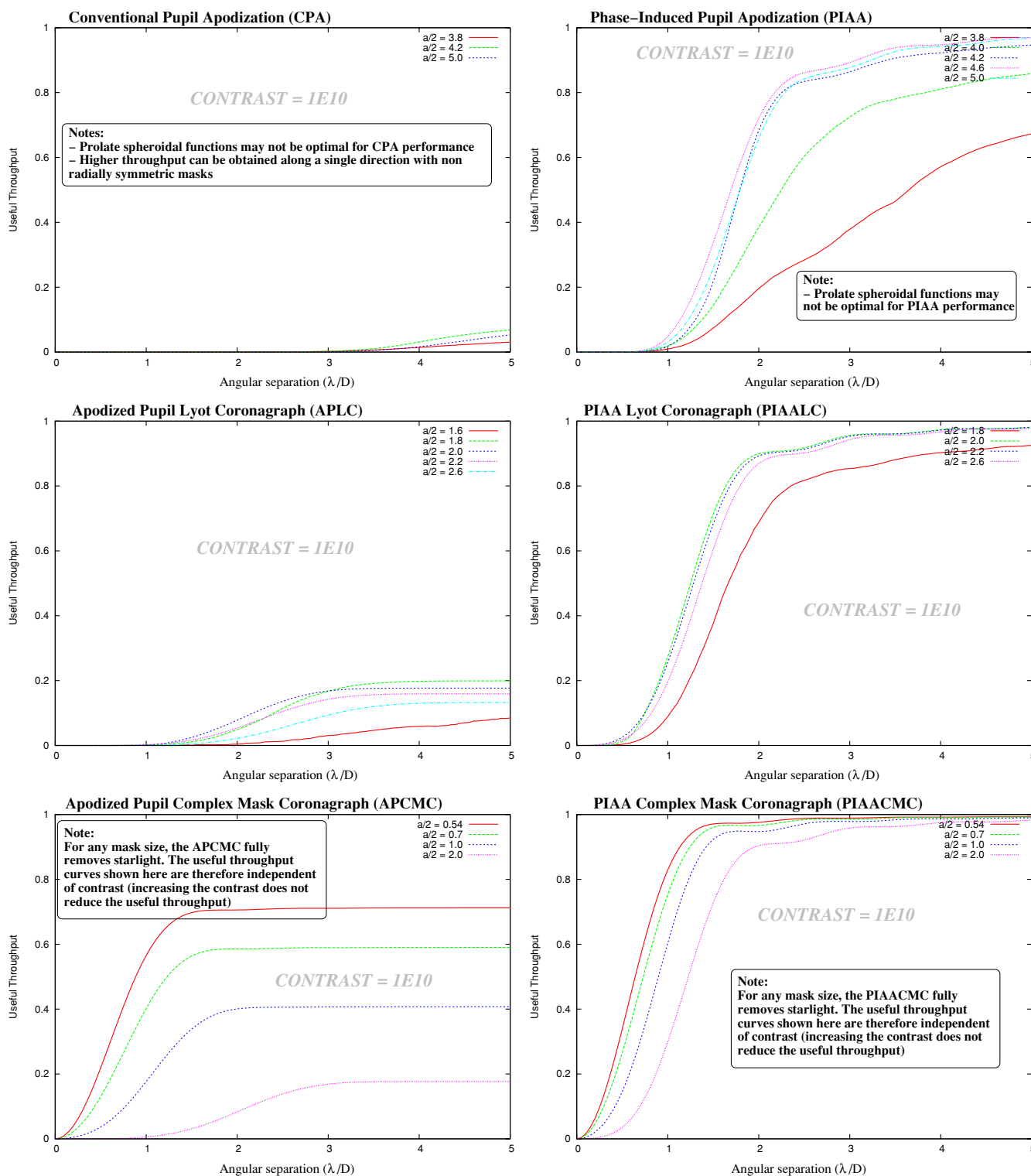
Figure 4. Performance of the six coronagraph architectures at the 10^{10} contrast level. The UT at 10^{10} contrast is plotted as a function of angular separation. In each configuration, coronagraphs designed with several values for the focal plane mask radius $a/2$ (in λ/D units) are shown.

(A color version of this figure is available in the online journal.)

3.2.4. Phase-shifting Focal Plane Masks: APCMC and PIAACMC

As described in Section 2.3, allowing the focal plane mask to be both partially transmissive and phase shifting enables perfect coronagraphic extinction for any focal plane mask radius $a/2$ above $0.54\,\lambda/D$. In the APCMC configuration, the coronagraphic extinction is therefore perfect for all mask sizes above $0.54\,\lambda/D$, and weaker apodizations/smaller focal plane

mask sizes than for the APLC configuration can be adopted. The performance curve is entirely driven by the focal plane mask size and is independent of contrast, as can be seen by comparing Figures 4 and 5. The highest performance APCMC is the one for which the focal plane mask is purely phase shifting (no absorption), which occurs for $a/2 \approx 0.54\,\lambda/D$ (exact value between 0.53 and 0.54), with a 73% apodization throughput.
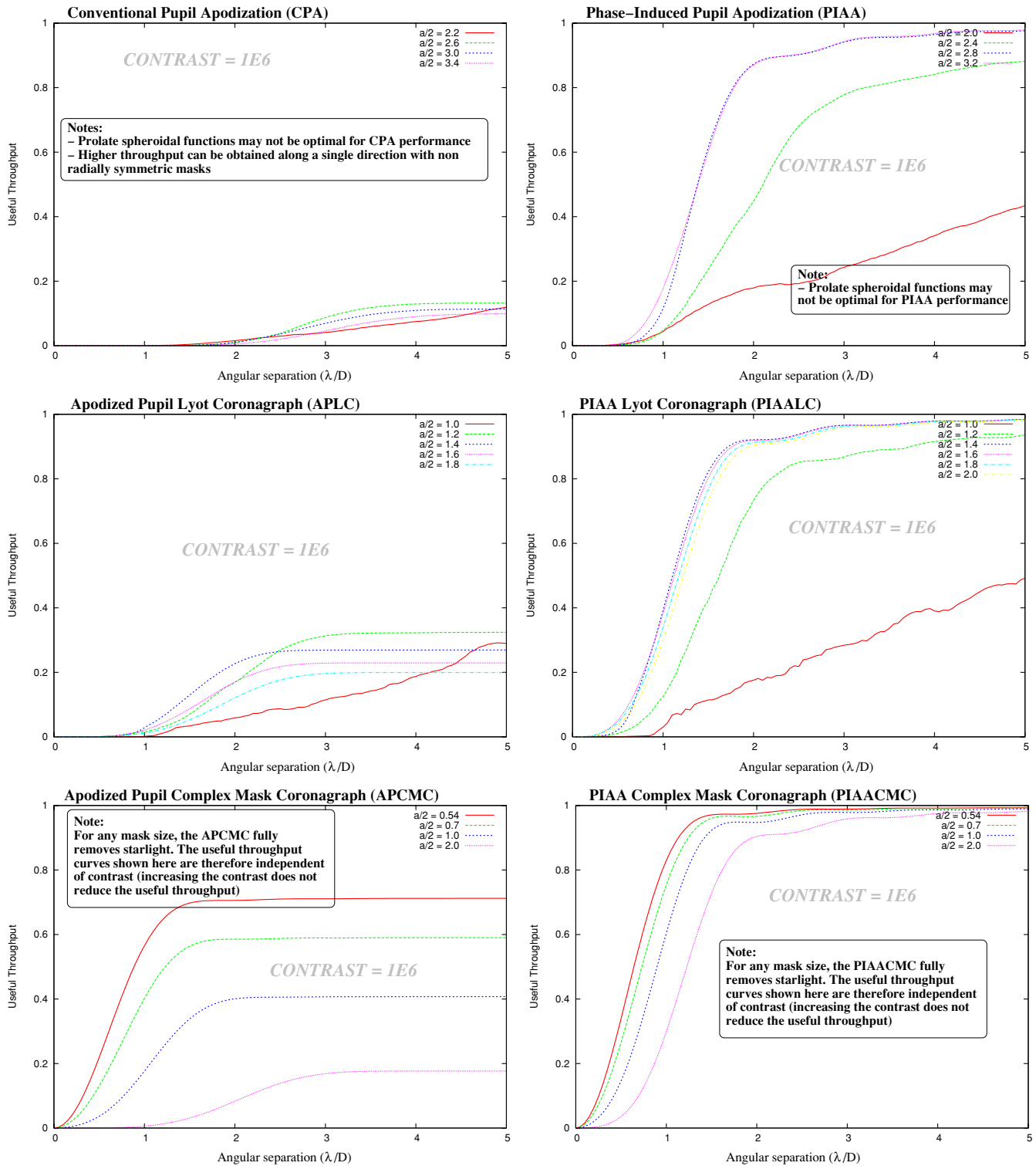
Figure 5. Performance of the six coronagraph architectures at the 10^6 contrast level. The UT at 10^6 contrast is plotted as a function of angular separation. In each configuration, coronagraphs designed with several values for the focal plane mask radius $a/2$ (in λ/D units) are shown.

(A color version of this figure is available in the online journal.)

With stronger apodizations, both the throughput and the IWA of the APCMC become poorer.

In the PIAACMC, the APCMC apodization-related losses in throughput and angular resolutions are removed. While the performance difference between the PIAACMC and APCMC is relatively small at the smaller focal plane mask size, it becomes larger as the focal plane mask radius increases. The PIAACMC performance decreases relatively slowly as the focal plane mask becomes larger and more opaque. As will be shown in Section 5, this is a fundamental advantage of the PIAACMC since the tolerance on focal plane mask phase shift errors is greatly relaxed for larger darker masks.

Table 1
PIAACMC Design Examples

Mask Radius $a/2$ (λ/D)	Eigenvalue Λ_0	Mask Transm t^2 [a]	Light Fraction on foc. Mask	Prolate Throughput [b]	Prolate Edge Value $\phi_a(1.0)$	IWA[c] (λ/D)
0.54	0.50830	93.6%	47.7%	71.6%	48%	0.64
0.70	0.69437	19.4%	67.0%	59.3%	30%	0.73
1.00	0.90428	1.12%	89.3%	40.8%	9.7%	0.90
1.50	0.99199	6.5×10^{-5}	99.1%	24.7%	0.86%	1.09
2.00	0.99948	2.7×10^{-7}	99.95%	17.7%	6×10^{-4}	1.23
3.00	0.999998	3.2×10^{-12}	99.9998%	11.4%	2.5×10^{-6}	1.47
4.00	0.999999995	2.4×10^{-17}	99.999988%	8.4%	9.3×10^{-9}	1.67

Notes.

[a] All focal plane masks are circular disks which introduce a π phase shift and attenuate light by the transmission given in this column.

[b] The prolate throughput is the throughput that a conventional apodizer would achieve for the prolate apodization at the input of the PIAACMC. In the PIAACMC, since the apodization is performed by beam shaping, the throughput of the apodization is 100%.

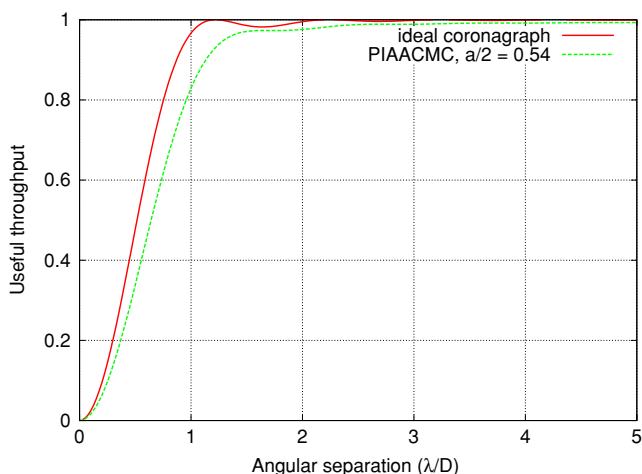[c] The inner working angle (IWA) is defined as the angular separation at which the throughput reaches 50%.

Figure 6. Comparison between the UT of the PIAACMC with $a/2 = 0.54\,\lambda/D$ (apodized pupil phase mask coronagraph) and the theoretical ideal performance limit of coronagraphy on a point source.
(A color version of this figure is available in the online journal.)

Figure 6 shows that the performance of a PIAACMC with a small $a/2 = 0.54\,\lambda/D$ almost pure phase-shifting $t \approx -1$ focal plane mask is close to the ideal coronagraph performance limit identified by Guyon et al. (2006) using first principles.

3.3. PIAACMC Design Examples

A few PIAACMC design examples are given in Table 1. The first example in this list is very close to an apodized pupil phase mask coronagraph: the focal plane mask is almost entirely phase shifting with a 93.6% transmission. The pupil apodization for this design is quite mild, and would only remove 28.4% of the light if it were done "classically." This design offers the best IWA (defined here as the 50% UT level): $0.64\,\lambda/D$.

As the focal plane mask size increases, it rapidly becomes opaque: at $a/2 = 1.0\,\lambda/D$, the mask intensity transmission t^2 is down to 1.12%, and at $a/2 = 2.0\,\lambda/D$, it is 2.7×10^{-7}. For mask sizes above $a/2 = 2\,\lambda/D$, the focal plane mask is so opaque that the PIAACMC becomes close to a PIAALC. Larger mask sizes increase the IWA, but this increase is quite slow thanks to the lossless apodization by the PIAA optics.

PIAACMCs block the central starlight in two steps:

1. First, a fraction of the starlight is blocked by the focal plane mask.

2. All of the remaining light is outside the pupil area, and is blocked by the Lyot mask in the pupil plane. Within the pupil area (inside the Lyot mask opening), the PIAACMC induces a destructive interference between the light that passed through the focal plane mask and the light that passed around it.

As the focal plane mask size $a/2$ increases, the relative contribution of these two effects changes. For small values of $a/2$, the coronagraph relies almost entirely on (2): the focal plane mask is transmissive and blocks little light. The focal plane size is then adjusted such that approximately half of the light passes through the mask (Table 1 shows that 47.7% of the light is phase shifted by the focal plane mask for $a/2 = 0.54$) and half the light passes around. There is a destructive interference in the Lyot plane, as shown in Equation (4) by the difference between the field corresponding to the image of the pupil and the field diffracted by the addition of the focal plane mask. This is true both for fully opaque masks and phase-shifting masks, but the interference is more efficient for phase-shifting masks (where $\epsilon > 1$). As the focal plane mask size increases, the contribution of effect (1) increases (the mask becomes opaque), and the focal plane mask captures a larger fraction of the incident light in order to keep the required balance between the phase-shifted light transmitted by the mask and the light outside the mask.

4. SENSITIVITY TO STELLAR ANGULAR SIZE

Guyon et al. (2006) showed that the theoretical performance limit a coronagraph can reach is a steep function of the source angular size. The PIAACMC is no exception to this fundamental rule, and the performance shown in Figure 6 rapidly degrades as the central source size increases. Figure 7 shows, for a 10^9 contrast and a $0.001\,\lambda/D$ radius source, that the UT reaches 50% just before $1.5\lambda/D$ instead of $0.65\,\lambda/D$ for a point source. In all simulations including source size shown in this paper, the source image is computed as the incoherent sum of 1256 coronagraphic PSFs corresponding to a regular square grid of points on the stellar surface.

Figure 7 shows that an aggressive PIAACMC design with a small $a/2 = 0.54\,\lambda/D$ focal plane mask radius does not perform as well as a more conservative design with a larger focal plane mask. From now on, we make a distinction between the coronagraph IWA, a fundamental property of the coronagraph design which is measured on a point source, and the practical
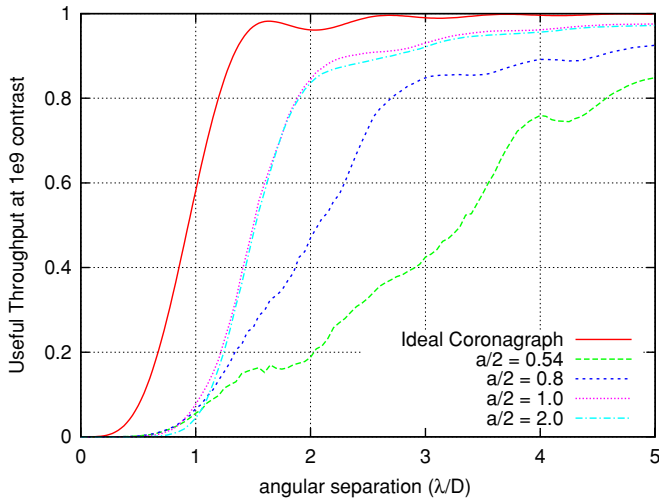
Figure 7. UT (*y*-axis) at 10^9 contrast is shown here as a function of angular separation (*x*-axis) for several values of the focal plane mask radius in a PIAACMC observing a partially resolved star of radius 0.001 λ/D. Unlike the bottom right panel of Figure 4, aggressive PIAACMC designs with small $a/2$ values perform poorly when the source is partially resolved.

(A color version of this figure is available in the online journal.)

Figure 8. Optimal PIAACMC focal plane mask size (*y*-axis) as a function of source radius (*x*-axis) for three contrast values between the star and the planet. The optimal mask size is the one for which the practical IWA achieved is the smallest. The irregular shape of the 10^9 contrast curve for source radius above $10^{-3} \lambda/D$ is due to the weak dependence of PIAACMC performance with focal plane mask size when $a/2 > 3 \lambda/D$.

(A color version of this figure is available in the online journal.)

IWA, which is the angular separation at which exoplanets can be detected when the stellar angular size is taken into account, is therefore a function of both the coronagraph design and the source observed. Both quantities are measured as the smallest angular separation for which the UT is equal to 50%. For any stellar angular radius value and goal contrast, there is an optimal focal plane mask size which minimizes the practical IWA. This optimal focal plane size is shown in Figure 8 as a function of source size for three contrast values between the star and the planet. In each case, the optimal mask size increases with source size. At a 10^5 contrast level, the most aggressive PIAACMC design ($a/2 = 0.54$) is optimal up to a $\approx 0.01 \lambda/D$ source radius, while at the 10^9 contrast level, $a/2$ should be increased to $\approx 1 \lambda/D$ even for the smallest source size considered in the figure (0.0001 λ/D radius).

While the increase in mask radius $a/2$ is significant in Figure 8 (up to a factor ≈ 6 over the minimum $a/2 = 0.54$ size), the corresponding loss in IWA is not always that large, as IWA is not linearly linked to the focal plane mask size thanks to the lossless PIAA apodization. For example, Table 1 shows that, for a point source, increasing the focal plane mask radius from 0.54 to 4.0 (more than seven-fold increase) results in a 2.6-fold increase in IWA. We examine in the next section how the PIAACMC practical IWA is a function of both contrast goal and stellar angular size.

4.1. PIAACMC Performance for Direct Imaging of Exoplanets

Figure 9 (bottom) shows how practical IWA is a function of source radius. The six curves shown correspond to different contrast levels ranging from 10^5 to 10^{10}. Each point in this figure corresponds to a PIAACMC design with the focal plane mask radius $a/2$ chosen to minimize the practical IWA. For comparison, the same curves are shown for PIAA (top), for which the size of the purely opaque focal plane mask was fixed at $a/2 = 4.6$. The curves show that the practical IWA in a PIAACMC can be much smaller than for PIAA as long as the contrast goal is moderate and/or the source is small.
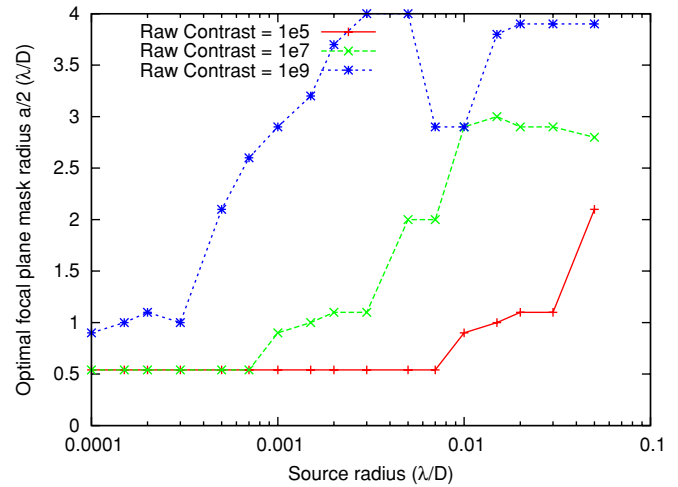
Table 2 gives for a few example observations of reflected light planets the value of the practical IWA achieved with a PIAACMC. In each case, the coronagraph goal "raw" contrast was set such that coronagraphic leaks due to stellar angular size are no more than 10 times the expected surface brightness of the planet PSF. This coronagraphic leak is incoherent and will not interfere constructively with speckles due to wavefront errors: the two terms add incoherently in intensity (not amplitude). It is also highly predictable since it is driven by a single parameter (the stellar angular size) and stable in time (assuming the coronagraph pointing is sufficiently sable). Its only contribution to detection limits is therefore photon noise. The factor 10 is chosen here somewhat arbitrarily, and a more complete sensitivity computation taking into account all sources of noise would need to be done to properly choose this factor. For most Earth-like planet targets embedded in an exozodiacal cloud similar to the one in the solar system, the background (zodiacal and exozodiacal light) surface brightness is expected to be approximately 10 times brighter than the planet's image: allowing for a similar stellar leaks to be at the same background level therefore has a moderate impact on detection limits. The practical IWA is also given in the table, under the same assumptions, for an ideally optimized PIAA coronagraph with full PIAA apodization (no conventional apodizer to mitigate the PIAA optics manufacturing challenges described in the next section).

Table 2 shows that for Jupiter-like planets (planet-to-star contrast = 10^9, required raw coronagraph contrast = 10^8), the PIAACMC practical IWA is 1.16 λ/D, which is 27.5% smaller than could be achieved with a PIAA coronagraph. The corresponding gain in the number of IWA-accessible targets is statistically expected to be a factor of 2.6, although actual detections would likely increase by a smaller factor due to other limitations (such as the limited total exposure time available to a mission and the slew+setup time to move to a new target). For Earth-like planets, the coronagraph performance is already limited by stellar angular size in a PIAA configuration, and the PIAACMC is unable to improve the practical IWA. The
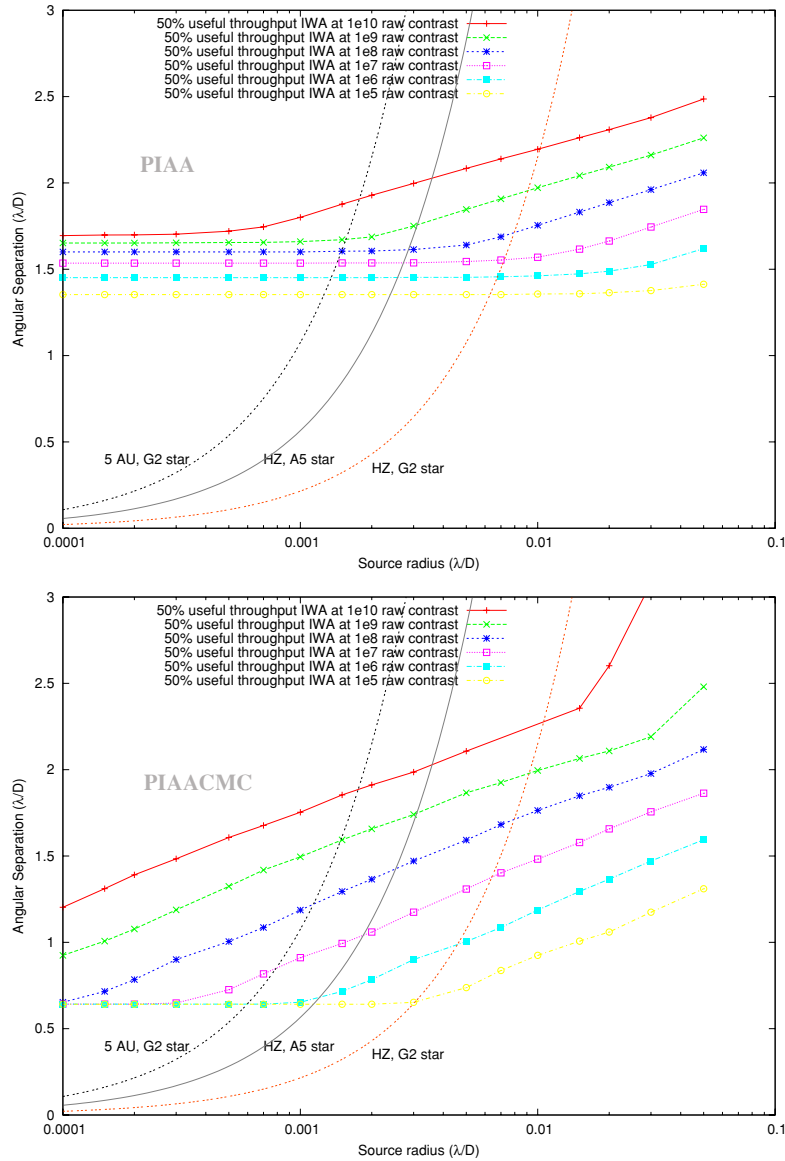
Figure 9. PIAACMC (bottom) offers smaller practical IWA than PIAA (top) if the central source radius (*x*-axis) is not too large and the contrast goal is not too extreme. In each plot, the IWA (defined here as the 50% UT point) is shown as a function of source radius (*x*-axis) for several contrast values. Curves showing angular separation vs. source radius are shown for three planet/star systems: a planet at 5 AU from a G2 main-sequence star and planets in the habitable zone (distance $= \sqrt{L_\odot}$ AU) of G2 and A5 main-sequence stars. Since the ratio between stellar angular size and star–planet angular separation is fixed in each of the three cases explored, these curves would be straight lines in a linear–linear scale but they appear curved in the log-linear scale adopted here. A point moves up and to the right along these curves as the telescope diameter increases, the observing wavelength decreases, or the distance to the system decreases. For example, the PIAACMC plot (bottom) shows that to reach a 10^7 raw contrast (purple curve) in the habitable zone of a G2 type main-sequence star, the habitable zone angular distance (dashed orange line) needs to be 1.4 λ/D or larger.

(A color version of this figure is available in the online journal.)

Table 2
"Practical" Inner Working Angles with PIAACMC for Reflected Light Planets
(Visible Light)

Planet Type	Star Type	Orbit Semi Major Axis	Raw Contrast	R_{star}/sep	Practical IWA 50% UT for 10x Planet Light PIAACMC	PIAA
Jupiter	G2	5 AU	1e-9	0.00093	1.16	1.60
Jupiter	G2	1 AU	2.5e-8	0.0047	1.17	1.51
Earth	G2	HZ = 1 AU	1e-10	0.0047	1.85	1.85
SuperEarth	G2	HZ = 1 AU	4e-10	0.0047	1.68	1.72
Jupiter	A5	HZ = 4.5 AU	1.25e-9	0.0018	1.29	1.60
Earth	A5	HZ = 4.5 AU	5e-12	0.0018	2.02	2.00
SuperEarth	A5	HZ = 4.5 AU	2e-11	0.0018	1.80	1.86

PIAACMC could enable detection of more Earth-like planets only if a large exposure time is allocated per target in order to recover planets fainter than the 1/10th stellar leak limit assumed in Table 2. The largest gain offered by PIAACMC is for ground-based imaging at $\approx 10^5$ raw contrast, where the practical IWA can be reduced to 0.64 λ/D.

5. MANUFACTURING TOLERANCES AND CHALLENGES

5.1. PIAA Optics

PIAA optics are highly aspheric and need to be manufactured to tight tolerances. The most challenging feature is the rapid decrease in radius of curvature at the edge of the first PIAA

element—this feature is necessary to spread the light at the outer part of the input beam into a wide area in the output beam. The rate at which curvature radius decreases and its minimum value are function of the "light dilution" the PIAA optics need to achieve at the edge of the beam, or, equivalently, the value of the apodization function at the edge of the beam.

In a conventional PIAA coronagraph, the edge of the apodized beam needs to be extremely dark to achieve high contrast, resulting in optics that are practically impossible to manufacture. Even if they could be manufactured to the required shape, the strongly curved narrow edge of the first PIAA element would introduce chromatic diffraction effects preventing high achromatic contrast (Vanderbei 2006). These problems are solved by sharing the apodization between the PIAA optics, which perform most of the apodization but leave the edge of the beam at some acceptably large brightness level, and a conventional apodizer which completes the apodization by darkening the edges of the beam (Pluzhnik et al. 2006). This approach has the double benefit of making the PIAA optics easier to manufacture, and of allowing larger-than-usual errors in the apodization mask since it only affects the faint edges of the beam. The apodizer is however responsible for a $\approx 10\%$ light loss and a $\approx 5\%$ increase of the planet's image size and the coronagraph IWA.

Several sets of reflective and refractive PIAA optics for high contrast imaging have been successfully manufactured for apodizations where the surface brightness at the edge of the beam is $\approx 1\%$ of the center surface brightness. As shown in Table 1, for PIAACMC designs with focal plane mask radius smaller than $a/2 = 1.5$, the edge-to-center surface brightness ratio is above 0.86%, and the apodization may therefore be entirely done with PIAA optics, without requiring a conventional apodizer and the efficiency loss which comes with it.

5.2. Focal Plane Mask

The PIAACMC requires a phase-shifting partially transmissive circular mask. Manufacturing such a mask to tight tolerances is challenging, especially when the mask needs to function in a finite spectral band. We quantify in this section what the tolerances are on the mask transmission, phase shift, and size. We consider three PIAACMC designs:

1. **Design 1** (line 7 in Table 1). A PIAACMC for direct imaging of Earth-like planets from space, optimized to deliver the smallest practical IWA at a 10^9 raw contrast on 0.005 λ/D-radius sources (for Sun-like stars smaller than this radius, an Earth equivalent is within λ/D of the star). For this design, $a/2 = 4.0 \, \lambda/D$, the IWA is 1.67 λ/D, and the "practical IWA," when taking into account the stellar angular size, is 1.85 λ/D.

2. **Design 2** (line 4 in Table 1). A PIAACMC for direct imaging of Jupiter-like planets from space, optimized to deliver the smallest practical IWA at a 10^8 raw contrast on 0.001 λ/D-radius sources (for Sun-like stars smaller than this radius, a Jupiter equivalent is within λ/D of the star). For this design, $a/2 = 1.5 \, \lambda/D$, the IWA is 1.09 λ/D, and the practical IWA, when taking into account the stellar angular size, is 1.16 λ/D.

3. **Design 3** (line 1 in Table 1). A PIAACMC for direct imaging of young massive planets in the near-IR from the ground, optimized to deliver the smallest practical IWA at a 10^5 raw contrast. This PIAACMC has a $a/2 = 0.54 \, \lambda/D$ mask

radius and a 0.65 λ/D IWA, and is insensitive to stellar angular size up to 0.003 λ/D radius.

5.2.1. Focal Plane Mask Transmission and Phase Shift

Focal plane mask transmission and phase errors lead to an incomplete destructive interference, within the opening of the Lyot mask, between the light components that pass through and around the focal plane mask. We denote δt the relative error in mask complex transmission and $\delta\phi$ the error in mask phase. The mask complex amplitude is therefore $t = t_a(1 + \delta t + i\delta\phi)$ with $-1 < t_a < 0$ the ideal mask complex transmission for focal plane mask diameter a. The residual complex amplitude in the PIAACMC exit pupil is therefore, according to Equations (5) and (4):

$$\Psi_C(r) = \Lambda_a(\delta t + i\delta\phi)\Psi_A(r). \tag{6}$$

Errors in focal plane mask transmission and phase therefore add incoherently, and produce identical light intensity distributions in the focal plane: a 1% relative error in mask transmission ($\delta t = 0.01$) is equivalent to a 0.01 rad error in mask phase ($\delta\phi = 0.01$).

5.2.2. Focal Plane Mask Size Tolerance

In a PIAACMC, the focal plane mask radius $a/2$ needs to be matched to the pupil apodization profile ϕ_a. Since the size of the mask (and its transmission) is adjusted to achieve a destructive interference, in the Lyot mask, between light passing through the focal plane mask and light passing around the focal plane mask, an error in focal plane mask radius will offset this balance and leave residual light within the opening of the Lyot mask.

5.2.3. Numerical Results

Figure 10 shows the result of numerical simulations where, for each of the three coronagraph designs, the performance with an ideal focal plane mask is compared to a "transmission error" case and a "mask radius error" case. Coronagraphic performance is evaluated as the UT versus angular separation when each coronagraph design is observing the source it was designed to observe (source radii of 0.005 λ/D, 0.001 λ/D, and 0 for designs 1, 2, and 3, respectively).

In PIAACMC design 1 ($a/2 = 4.0$), almost all of the light is blocked directly by the focal plane mask. As shown in Table 1, the focal plane mask in this design is practically opaque (intensity transmission $t^2 = 2.4 \times 10^{-17}$), and all but $\approx 10^{-8}$ of the starlight falls on the mask. This design, optimized for detection of Earth-like planets, if very insensitive to errors in mask phase shift and very robust against errors in mask size: as shown in Figure 10, a 10% error in mask size leads to no appreciable loss in performance. Since the mask is almost opaque ($t^2 = 2.4 \times 10^{-17}$), a large relative error on its transmission will not have an effect on coronagraphic performance: for a 10^{-10} contrast detection, an increase of the mask transmission by six orders of magnitude will not affect detection.

PIAACMC design 3, although it is optimized for a more moderate contrast (10^5), is the most sensitive to focal plane mask transmission errors. A 1% error in mask amplitude transmission is sufficient to reduce the coronagraph performance (see Figure 10). This is due to the fact that the mask is almost transparent, and a small relative error in mask transmission therefore corresponds to a large absolute error in light transmitted by the mask. This PIAACMC design is also sensitive to mask size, although not quite as much as PIAACMC design 2.
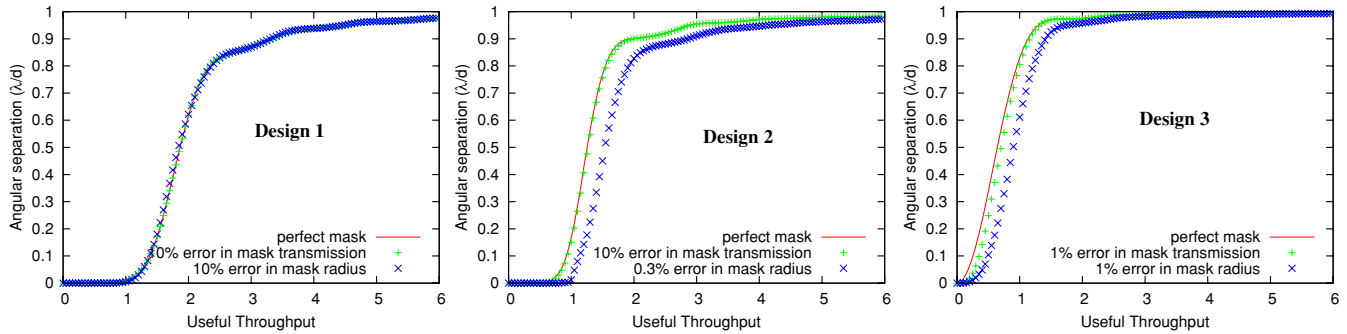
Figure 10. Effect of focal plane mask mismatch, in transmission and radius, on the coronagraphic performance for three example observations. As described in Section 5.2.1, the impact on performance from a 1% error in mask throughput (0.5% in mask complex amplitude) is equivalent to a 0.005 rad = 0°.3 error in mask phase shift.

(A color version of this figure is available in the online journal.)

5.2.4. Mask Design for Achromatization

The PIAACMC focal plane mask manufacturing is likely to be challenging, and will place strong constraints on the PIAACMC design. While a quantitative assessment of the manufacturing challenges and capabilities is beyond the scope of this paper, we outline the most challenging requirements for the mask and point to possible technical approached to mitigate them.

The PIAACMC focal plane mask needs to be manufactured with appropriate transmission and a phase shift across the observation spectral bandwidth. While ideally, the phase shift should be π and the transmission should follow the transmission given in Figure 3, large focal plane masks ($a/2 > 2\lambda/D$) can be made purely opaque with no loss in coronagraph performance. With a purely opaque focal plane mask, the coronagraph becomes a PIAA Lyot Coronagraph (PIAALC), which is an apodized pupil Lyot coronagraph in which the apodization is performed with PIAA optics. For direct imaging of Earth-like planets around nearby stars from space with a telescope sufficiently large to partially resolve stellar disks, the PIAACMC therefore does not offer performance enhancement over a PIAALC, as the achievable performance is limited by the stellar angular size and the masks required have such a low transmission that they can be replaced by a purely opaque mask with no change in coronagraph performance. As the focal plane mask becomes smaller, its phase shift and transmission need to be better controlled, as illustrated by the analysis performed in Section 5.2.3. Both phase shift and transmission may be tuned by multi-layer coating designs. Transmission may also be reduced by lithographic deposition of a small regular grid of opaque dots, or holes in an otherwise opaque coating (the size of such features should probably be larger than λ to minimize chromatic diffractive effects and much smaller than $f\lambda/D$ to be seen as a smooth feature from within the Lyot pupil mask opening). Assuming that the hole size should be at least 10λ to minimize chromatic effects, with an F-number equal to 100 and 100 dots per diffraction limit on the mask (10 dots linearly per $f\lambda/D$), the minimum transmission in t^2 is 10^{-2}. The microdot technique therefore cannot be used by itself to achieve low transmissions polychromatically, and needs to be combined with other techniques such as conventional filtering. A detailed analysis of the chromatic behavior of transmission should be performed for any mask designed, but is outside of the scope of this paper.

The most challenging requirement is the mask size, which needs to scale proportionally with λ. Several possible options exist to address this problem:

1. A refractive achromatizer (Wynne 1979) can be placed after the PIAA optics to scale the pupil size as $1/\lambda$. We note that refractive optics would likely introduce wavelength-dependent aberrations which are very hard to correct with deformable mirrors. This solution, even if carefully designed, may therefore only be applicable to systems designed for moderate contrast, such as ground-based coronagraphs designed to deliver 10^{-4} to 10^{-6} raw contrast.
2. A chromatic mask could be placed in a pupil plane before or after the PIAA optics to perform a wavelength-dependent apodization. The apodization would be stronger (produce a smaller pupil) in the blue and milder (produce a larger pupil) in the red. This scheme could produce the same pupil wavelength dependence as the refractive achromatizer option listed above, but will result in a loss of throughput in the blue side of the band. We note that manufacturing of this apodizer to high precision may be challenging.
3. Chromatic effects could be mitigated directly at the focal plane mask, where a combination of coatings and zones would produce a mask which, as seen by the pupil opening in the Lyot stop, is bigger in the red than in the blue. This approach offers sufficient flexibility to also provide the wavelength-independent transmission and phase required. A simplified version of this scheme, using only two zones, was shown to provide significant improvement for phase mask coronagraphs (Soummer et al. 2003b).

These possible solutions have not been explored in this work, and we note that they would likely face manufacturing challenges that may limit their usefulness to either moderate contrasts or relatively large focal plane mask size ($a/2$) values.

6. CONCLUSION

The PIAACMC is an attractive high performance alternative to PIAA when the contrast goal and source angular size allow IWAs smaller than $\approx 2.0\lambda/D$. The PIAACMC concept is therefore especially powerful for ground-based coronagraphic imaging targeting young massive planets and disks, where it enables detection within $1\lambda/D$ separation. By reducing the IWA to less than $1\lambda/D$ at no cost in sensitivity, the PIAACMC also brings reflected light planets within the capture range of current ground-based telescope, although such targets require a challenging 10^7 detection contrast limit. PIAACMC is also well suited for direct reflected light imaging of Jupiter sized exoplanets from space. The contrast/angular separation combinations for such planets allow the PIAACMC to push

the "practical IWA" $\approx 25\%$ lower than could be achieved with an optimally designed PIAA coronagraph, therefore offering ≈ 2.5 times more targets (the number of accessible targets goes as IWA^{-3}). For direct imaging of Earth-like planets from space, the PIAACMC does not however offer a performance enhancement over an ideally designed PIAA coronagraph, as the achievable performance is limited by the stellar angular size.

The PIAACMC design offers the ability to tune the coronagraph IWA optimally for each observation, according to the angular size of the star and the goal contrast. For a space coronagraphic telescope designed to image a planet ranging from Earth-like to Jupiter-like around a sample of stars (each with its own angular diameter), it would be advantageous to be able to change the coronagraph parameters between observations. This would require a selectable focal plane mask and a selectable apodizer after the PIAA optics.

REFERENCES

Aime, C. 2005, A&A, 434, 785
Aime, C., Soummer, R., & Ferrari, A. 2001, A&A, 379, 697
Belikov, R., Kasdin, N. J., & Vanderbei, R. J. 2006, ApJ, 652, 833
Gonsalves, R., & Nisenson, P. 2003, PASP, 115, 706
Guyon, O. 2003, A&A, 404, 379
Guyon, O., Matsuo, T., & Angel, R. 2009, ApJ, 693, 75

Guyon, O., Pluzhnik, E. A., Galicher, R., Martinache, F., Ridgway, S. T., & Woodruff, R. A. 2005, ApJ, 622, 744
Guyon, O., Pluzhnik, E. A., Kuchner, M. J., Collins, B., & Ridgway, S. T. 2006, ApJS, 167, 81
Guyon, O., & Roddier, F. 2000, in Darwin and Astronomy: the Infrared Space Interferometer, ed. B. Schürmann (ESA-SP 451; Noordwich: ESA), 41
Jacquinot, P., & Roisin-Dossier, B. 1964, Prog. Opt., 3, 29
Kasdin, N. J., Vanderbei, R. J., Spergel, D. N., & Littman, M. G. 2003, ApJ, 582, 1147
Lagrange, A.-M., et al. 2009, A&A, 493, L21
Marois, C., Macintosh, B., Barman, T., Zuckerman, B., Song, I., Patience, J., Lafrenière, D., & Doyon, R. 2008, Science, 322, 1348
Martinache, F., Guyon, O., Pluzhnik, E. A., Galicher, R., & Ridgway, S. T. 2006, ApJ, 639, 1129
Nisenson, P., & Papaliolios, C. 2001, ApJ, 548, L201
Pluzhnik, E. A., Guyon, O., Ridgway, S. T., Martinache, F., Woodruff, R. A., Blain, C., & Galicher, R. 2006, ApJ, 644, 1246
Roddier, F., & Roddier, C. 1997, PASP, 109, 815
Soummer, R. 2005, ApJ, 618, L161
Soummer, R., Aime, C., & Falloon, P. E. 2003a, A&A, 397, 1161
Soummer, R., Dohlen, K., & Aime, C. 2003b, A&A, 403, 369
Soummer, R., Pueyo, L., Ferrari, A., Aime, C., Sivaramakrishnan, A., & Yaitskova, N. 2009, ApJ, 695, 695
Traub, W. A., & Vanderbei, R. J. 2003, ApJ, 599, 695
Vanderbei, R. J. 2006, ApJ, 636, 528
Vanderbei, R. J., Kasdin, N. J., & Spergel, D. N. 2004, ApJ, 615, 555
Vanderbei, R. J., Spergel, D. N., & Kasdin, N. J. 2003, ApJ, 599, 686
Vanderbei, R. J., & Traub, W. A. 2005, ApJ, 626, 1079
Wynne, C. G. 1979, Opt. Commun., 28, 21